PCCP

Accepted Manuscript

This is an *Accepted Manuscript*, which has been through the Royal Society of Chemistry peer review process and has been accepted for publication.

Accepted Manuscripts are published online shortly after acceptance, before technical editing, formatting and proof reading. Using this free service, authors can make their results available to the community, in citable form, before we publish the edited article. We will replace this *Accepted Manuscript* with the edited and formatted *Advance Article* as soon as it is available.

You can find more information about *Accepted Manuscripts* in the Information for Authors.

Please note that technical editing may introduce minor changes to the text and/or graphics, which may alter content. The journal's standard Terms & Conditions and the Ethical guidelines still apply. In no event shall the Royal Society of Chemistry be held responsible for any errors or omissions in this *Accepted Manuscript* or any consequences arising from the use of any information it contains.

ROYAL SOCIETY OF CHEMISTRY

www.rsc.org/pccp

Oxygen Reduction and Oxygen Evolution in DMSO Based Electrolytes: Role of the Electrocatalyst

C. J. Bondue[a], P. Reinsberg[a], A. A. Abd-El-Latif[a,b], H. Baltruschat[a]*

[a] Institut für Physikalische und Theoretische Chemie, Universität Bonn, Römerstraße 164, D-53117 Bonn, Germany

[b] On leave of absence from the National Research Centre, Physical Chemistry Dept., El-Bohouth St. Dokki, 12311 Cairo, Egypt.

Abstract

In the present paper the role of the electrode material on oxygen reduction in DMSO based electrolytes is elucidated using DEMS. We have found, employing platinum, gold, ruthenium rhodium, selenium decorated rhodium and boron doped diamond (BDD) as electrode materials, that the actual mechanism of oxygen reduction largely depends on the electrode material. At platinum, rhodium and selenium decorated rhodium the final reduction product, peroxide, is formed electrochemically. At gold and at low overpotentials oxygen is reduced to superoxide and peroxide is only formed by disproportionation of the latter. No oxygen reduction takes place at the diamond surface of the BDD-electrode, hence, showing unambiguously that oxygen reduction is an inner sphere reaction. Also, the rate of oxygen evolution varies with the electrode material, although the onset potential of oxygen evolution is not influenced. The amount of peroxide formed is limited to 1 – 2 monolyers. Contrary to intuition oxygen reduction and oxygen evolution from peroxide, therefore, are heterogeneous, electrocatalytic reactions. The finding of such an electrocatalytic effect is of great importance for the development and optimization of lithium air batteries. Aside from the electrode material there are also effects of water as well as of the cation used in the electrolyte. This suggests an influence of the double layer at the interface between the electrode and the electrolyte on oxygen reduction in addition to the well-known higher stability of Na_2O_2 and K_2O_2. Electrospray ionization (ESI) results show that any effect of water in Li^+ containing electrolyte is not due to an altered solvation of the cation.

Introduction

In 1996 Abraham introduced the concept of lithium air batteries with a theoretical specific energy density of 18.7 kJ/g based on the discharged battery and assuming Li_2O as the final discharge product[1]. Since then a lot of effort was put into research related to lithium air batteries, mainly because the construction of a secondary battery with such capacities would certainly pose a large leap forward in electrifying automotive traffic[2-5]. It is established now that oxygen reduction in various organic electrolytes is not reduced to Li_2O but forms Li_2O_2 instead[6-9,10]. Discharge to Li_2O_2 reduces the theoretical capacity of the battery to 13.8 kJ/g. This was calculated from thermodynamic data[11, 12]. Only 90.2% of that energy can be harnessed, while the remaining 10% are lost to entropic heat flow. Even though discharge to Li_2O_2 (instead of Li_2O) reduces the theoretical energy density of lithium air batteries, they continue to raise attention.

In lithium air batteries employing ether based electrolytes some authors described the formation of toroid shaped Li_2O_2 particles upon discharge at low current density, whereas no such particles were found when large current densities were applied[13-15]. However, under similar experimental conditions other authors did not observe the formation of toroide shape

particles[15, 16]. Although it was recently suggested that the difference observed in literature might be due to different water contents of the electrolyte, with water favouring the formation of toroide shape particles, the growth mechanism of Li_2O_2 remains poorly understood[17, 18]. A proposed mechanism involves the LiO_2 mediated dissolution and re-deposition of Li_2O_2 with water facilitating the formation of soluble LiO_2[17]. Others proposed the formation of LiO_2 as an intermediate of oxygen reduction, that adsorbs with higher probability at certain sites where it is reduced[19].

All model batteries reported in literature so far suffer from large charging overpotentials. Because of that some authors employed precious metals[20, 21,22] or transition metal oxides[23-25] in the oxygen electrode in order to reduce the charging potential. Given that the batteries in these studies employed carbonate based electrolytes the claimed catalytic effect is most probably due to enhanced kinetics of oxidation of decomposition products rather than enhanced kinetics of Li_2O_2 oxidation[23, 24].

Nevertheless, the choice of the electrode material for the gas diffusion electrode seems to have an effect on the cycleability of a lithium oxygen battery. Marinaro *et al*. found that batteries employing an oxygen electrode made from gold sputtered Super-P could be cycled 5 times more often than a battery that featured an oxygen electrode without any gold coating. In addition Marinaro *et al*. found that the Au/Super-P electrode could sustain larger current densities upon discharge[26]. A similar superior performance of an Au/Super-P electrode over a Super-P electrode was found by the same group in a battery featuring a tetraglyme based electrolyte[27].

Beside the construction of model batteries also fundamental research on oxygen reduction has been done[7, 10, 17, 22, 28-36]. It was found that the current density for oxygen reduction in ether based electrolytes depends on the electrode material. Lu *et al*. found a volcano like behaviour when the potential at which a given current density was observed is plotted against the binding energy of oxygen at the given electrode material[22].

Laoire *et al*. reported both on the effect of cations and on the effect of the solvent on oxygen reduction[28,7]: Oxygen reduction leads to the formation of peroxide in the presence of hard and small cations like Li^+, while in electrolytes containing soft and large cations, such as TBA^+, oxygen is reduced to superoxide[28]. Lithium superoxide is known only in the Argon matrix[37] and disproportionates to lithium peroxide and oxygen under ambient conditions. Therefore, it is not surprising that oxygen reduction in lithium containing electrolytes leads to the formation of Li_2O_2. The account for the somewhat larger Na^+ cation is more mixed. Both NaO_2 and Na_2O_2 are meta stable and known to exist. Laoire *et al*. proposed the formation of Na_2O_2 in an acetonitrile based and sodium containing electrolyte during oxygen reduction[28]. Also in some sodium oxygen batteries Na_2O_2 was found as the final discharge product[38-40], while others convincingly showed the formation of NaO_2 under similar experimental conditions in their batteries[41, 42]. So far it is entirely unknown under which conditions NaO_2 is formed and under which Na_2O_2[42].

To understand when and why oxygen reduction results in Na_2O_2 it seems helpful to turn to Li_2O_2 where there is more knowledge available on its formation process. There are two conceivable pathways to Li_2O_2: Via the indirect pathway superoxide is formed electrochemically and then undergoes Li^+-induced disproportionation in the aftermath. Via the direct pathway oxygen accepts two electrons from the electrode and forms peroxide electrochemically. Indeed Laoire *et al*. found superoxide as an intermediate in a lithium containing DMSO based electrolyte[7] during oxygen reduction. However, no indication for superoxide was found in acetonitrile based electrolytes. Laoire *et al.* ascribed this difference to the higher donor number of DMSO of 125 kJ/mol as compared to that of acetonitrile with 58.9 kJ/mol[43] allowing for a better solvation of Li^+ in DMSO and therefore for a longer lifetime of superoxide[7]. Also, others observed the formation of superoxide in DMSO based

electrolytes: Cao *et al.* employing spin traps showed the presence of superoxide by means of EPR [44]. During RRDE experiments in Li^+-containing, DMSO based electrolytes positive currents were observed at the ring electrode that were ascribed to the oxidation of superoxide[29, 31]. Based on the evaluation of CV data by the Nicholson and Shain relationship Laoire *et al.* proposed that at higher overpotentials peroxide is formed electrochemically while at lower overpotentials peroxide is formed indirectly by disproportionation of superoxide[7].

Experimental

Chemicals

All electrolytes were prepared in an *MBraun* glove box. During electrolyte preparation the humidity in the glove box atmosphere never exceeded 0.6 ppm. After preparation the electrolyte was kept in a sealed vessel and stored inside the glove box. The electrolyte was used within a time span of one week. The water content of the as prepared electrolyte did not exceed 13 ppm (with the exception of the Mg^{2+} containing electrolyte, which had a water content of ~50 ppm). During transfer the electrolyte gathered water in the single digit ppm-range.

Extra dry DMSO (99.7%, over molecular sieve, Acros Organics), $LiClO_4$ (battery grade, Sigma-Aldrich), highly pure lithium trifluoromethanesulfonate (LiTfO) (Sigma-Aldrich, ≥ 99.995%) Acetic Acid (KMF, 96%) and methanol (Fluka, 99.9%) were used as received. Sodium perchlorate (p.a., Fluka) and potassium perchlorate (99%, Sigma Aldrich) were dried at 180° C under reduced pressure, while magnesium perchlorate (p.a. Sigma-Aldrich) was dried at 245° C. Highly pure Ar (Air Liquid, 99.999%) was used for purging the electrolyte and highly pure nitrogen (Air Liquid, 99.9995%) was used as Auxiliary and Sheath gas in ESI experiments to facilities the evaporation of solvents. A custom made mixture of argon and oxygen (Ar : O_2 = 80 : 20) was obtained from Air Liquid.

A coulometric KF Titrator (C20, Metler Toledo) with a diaphragm electrode was used to determine the water content. The sample was taken at the outlet of the dual thin layer cell, hence, giving the water content after the measurement was completed. According to the manufacturer of the used electrolyte accumulation of DMSO affects the chemistry involved in the detection process of water. The error was estimated by adding a water standard. The water contents given in this article already account for the error of up to 30%.

BDD-electrodes were purchased from Adamant La-Chaux-de-Fonds, Switzerland. The electrode consisted of a layer of 1 µm diamond doped with 6000 ppm boron on a 1 mm thick silicon wafer.

Dual Thin Layer Cell

In the dual thin layer cell the electrolyte flows into the first compartment where the working electrode is placed. Reaction products are flushed along with the electrolyte into the second compartment where a porous Teflon membrane is pressed on a steal frit. Volatile reaction products evaporate through the Teflon membrane into the vacuum of the mass spectrometer. The electrolyte then is flushed to the outlet. The flow of the electrolyte going from the upper to the lower compartment causes a delay between the faradaic current and the response in the ionic current. In all calculations where the ionic current was correlated to processes appearing at the working electrode this delay time was accounted for.

The reference electrode is placed at the inlet. The main counter electrode is placed at the outlet. In order to reduce electronic oscillations, a second counter electrode is placed at the inlet. The main counter electrode is connected via a resistance of 1 Ω, the second via a 1 MΩ resistance to ascertain an optimal distribution of the current.

A more detailed description of the dual thin layer cell along with its versatile applications for DEMS can be found elsewhere[45-49].

Calibration for O_2

In order to correlate the ionic current observed by mass spectroscopy to the faradaic current calibration is required. To account for the collection efficiency of the dual thin layer cell electrochemical calibration with a reaction of known stoichiometry is required.

Calibration was done on the same day as the experiment by reducing oxygen from an electrolyte of 0.5 M $KClO_4$ in DMSO where at low overpotentials superoxide is formed. This potential region was identified by comparing the results to oxygen reduction in an electrolyte of 0.5 M $TBAClO_4$ in DMSO, where oxygen reduction is known to proceed via the formation of superoxide[50,7, 28]. We avoided calibration with $TBAClO_4$ in order to reduce costs and errors. The latter arise when the used $TBAClO_4$ contains impurities, noticeable by electrochemical side reactions at potentials close to the onset potential of oxygen reduction. The extent of impurities seem to depend on the manufacturer and the charge.

Reference Electrode

The reference electrode used in this study was a silver wire immersed in a solution of 0.1 M $AgNO_3$ in DMSO. Electrolyte contact to the working electrode was achieved by filling a Teflon tube with the silver containing solution and sealing it with a rough glass bead. The end with the glass bead was immersed into the working electrolyte, while the other open end was immersed into the silver containing solution. A drawing of the reference can be found elsewhere[50].

According to the values given by Gritzner *et al.*[51] the reference electrode described above has a potential of +3.89 V with respect to the Li^+/Li couple.

Determination of the Roughness Factor and Electrode Preparation

Prior to the experiment in the organic electrolyte all electrodes were cycled in deaerated 0.5 M sulphuric acid until no changes in the CV were observed. From these CVs the roughness factor (RF) of the gold electrodes were determined by integrating the region of oxide formation in the potential range from 1.36 to 1.78 V (vs. RHE) following the method described by Trasatti and Petrii[52]. The roughness factor of the platinum electrodes was determined by integrating the current due to H-upd in the potential region from 0.07 to 0.35 V (vs. RHE), in which 77% of a monolayer are formed[52]. Also for rhodium the true surface area was determined from the charge due to H-upd (0.25 V to 0.0 V)[53]. The true surface area of the ruthenium electrode was determined following the method described by Nagel *et al.* from the charge due to the dissolution of a monolayer of copper[54]. Given that there is no easy approach to determine the true surface area of the other electrode materials (glassy carbon, boron-doped diamond (BDD)) all current densities are given with respect to the exposed geometric surface area of 0.283 cm^2.

The Au(111)-electrode was prepared by the method described by Clavilier *et al.*[55] for platinum single crystals. The Au(111) single crystal was flame annealed and was allowed to cool down to room temperature in an argon atmosphere. The crystallinity of the surface was checked by recording a CV in 0.5 M sulphuric acid. Before transferring the gold crystal to the dual thin layer cell the electrode was rinsed with water. Droplets of water attached to the crystal were carefully removed by a lint-free laboratory wipe.

Prior to selenium deposition the rhodium electrode was flame annealed and was allowed to cool down in an atmosphere of argon and hydrogen (approximately 20% H_2) in order to

remove any surface oxide. This electrode then was transferred with a droplet of H_2-saturated water attached to its surface to a cell, where selenium was deposited by a potential sweep to 0.6 V (vs. RHE) in an electrolyte of 0.1 M $HClO_4$ containing 10^{-3} M SeO_2 [56]. From the charge passed during Se-deposition, and assuming that per Se 4 electrons are passed, the surface coverage of selenium was determined to be 0.72 ML (1 ML (= mono layer) is defined here as one Se-atom per Rh-surface atom).

Some reactions were shown to be sensitive to the surface termination of the BDD-electrode[57]. Therefore, in the present study experiments at the BDD-electrode were performed both with oxygen and hydrogen terminated surfaces. In order to prepare an oxygen terminated BDD-surface (BDD_{ox}) the electrode was swept to 2.5 V versus RHE in 0.5 M H_2SO_4 and was kept there for at least 10 minutes. The hydrogen terminated surface (BDD_{red}) were prepared by polarisation of the electrode to -1 V versus RHE in 0.5 M H_2SO_4 for at least 10 minutes.

ESI measurements

ESI-MS measurements were performed in the positive electrospray ionization mode on a Finnigan MAT SSQ7000 instrument at 4.5 kV and a capillary temperature of 250°C. The sample solution in gas-tight syringe (Hamilton) was introduced to the ESI system via 125 µm inner diameter PEEK tube at a flow rate 20 µl/min using a syringe pump (Syringe Infusion Pump 22, Harvard Apparatus, Inc., Cambridge, MA).

Results and Discussion

Oxygen Evolution

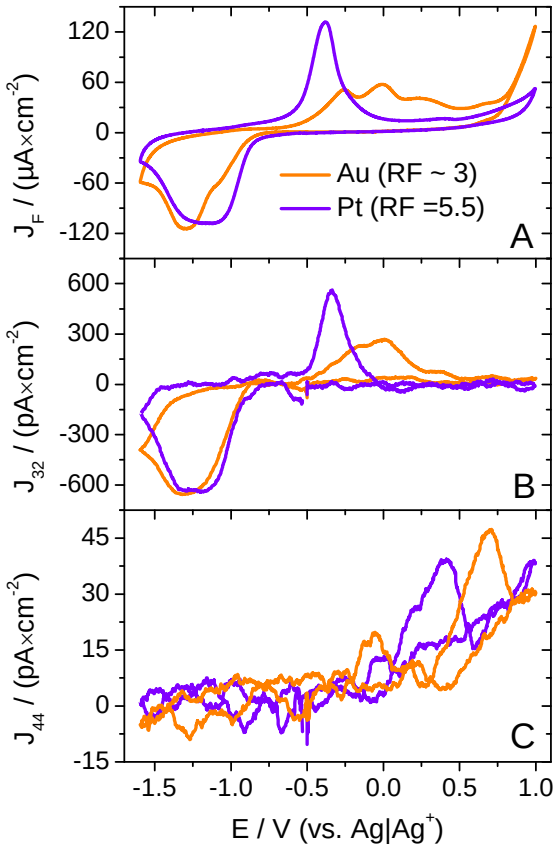

Figure 1: 1st CV (A) and 1st MSCV for mass 32 (B) and mass 44 (C) in an electrolyte of 0.5 M $LiClO_4$ in DMSO purged with a mixture of argon and oxygen (Ar : O_2 = 80 : 20); Sweep rate: 10 mV/s; Flow rate:

5µL/s; orange: At a gold electrode (RF~3); Purple: At a platinum electrode (RF = 5.5). Current densities are given with respect to the geometric surface area.

We have investigated the electrochemistry of oxygen reduction and oxygen evolution in an electrolyte of 0.5 M $LiClO_4$ in DMSO at a variety of electrode materials. Prior to the evolution of any oxygen in the anodic sweep, Li_2O_2 must be deposited on the electrode in a preceding cathodic sweep. However, for a better flow of reading we choose to discuss the oxygen evolution first. Figure 1 shows the CV and MSCV for mass 32 and 44 at those materials with the most striking differences in the potential region of oxygen evolution: Gold and platinum. In the experiment of Figure 1 and all other DEMS experiments discussed in this report several cycles were recorded. More than one cycle is only shown when differences appeared. In the measurements of Figure 1 this was not the case. In order to achieve a large response, especially in the MSCV for mass 32 during oxygen evolution, electrodes with a relatively high roughness factor were used (Pt: RF = 5.5; Au: RF ~ 3). Figure 2 shows the CV and MSCV for mass 32 and 44 obtained under the same experimental conditions as those in Figure 1 at rhodium, ruthenium and glassy carbon.

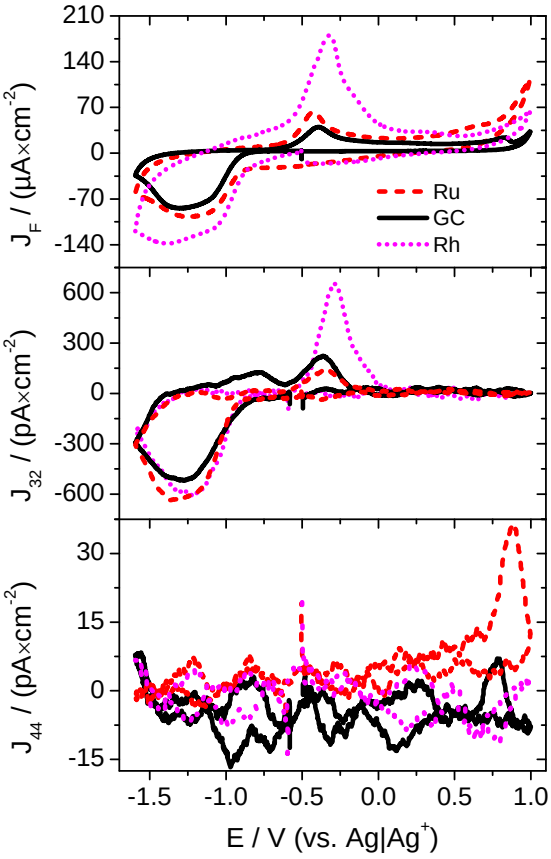

Figure 2: 1st CV (A) and 1st MSCV for mass 32 (B) and mass 44 (C) in an electrolyte of 0.5 M $LiClO_4$ in DMSO purged with a mixture of argon and oxygen (Ar : O_2 = 80 : 20); Sweep rate: 10 mV/s; Flow rate: 5µL/s; Red/dashed: At a ruthenium electrode; magenta/dotted: At a rhodium electrode; black/solid: At a glassy carbon electrode. Current densities are given with respect to the geometric surface area.

It is clear, both from the CV and the MSCV for mass 32 that oxygen evolution takes place in two distinguishable waves at the gold electrode. This is different at the platinum electrode where oxygen evolution proceeds in a single peak. Indeed among the electrode materials under investigation the gold electrode is unique in this regard as Figure 2 shows. The current density, based on real surface area, at the peak potential of -0.4 V is 24 µA/cm² at the platinum electrode. At the gold electrode the largest current density of 17 µA/cm² is observed at -0.25 V. Not only is the current density at platinum higher than at the gold electrode, but it

is also achieved at a lower overpotential. There are 2.2 nmol/cm^2 platinum atoms and 2.5 nmol/cm^2 gold atoms in the surface of the respective electrodes. From that we calculate a Li_2O_2 coverage of 1 ML at the platinum electrode and of 2 ML on the gold electrode. (In a previous report we have determined 3 monolayer of Li_2O_2 from the amount of reduced oxygen, however, from the amount of evolved oxygen, a coverage of only 1.7 monolayer is calculated (*c.f.* Table 1)[50].) The appearance of two distinguishable peaks in the potential region of oxygen evolution at gold suggests that the first monolayer of Li_2O_2 is thermodynamically more stable than the second. Differently from what was proposed by Albertus *et al.*[58], the charge transfer is not limited by the resistance of Li_2O_2 since oxygen evolution is the reaction of a mono- or biatomic surface layer of Li_2O_2. The different kinetics at the different electrodes clearly indicates a catalytic effect on the charge transfer. However, non of the electrode materials under review have an effect on the onset potential of oxygen evolution which is at -0.67 V.

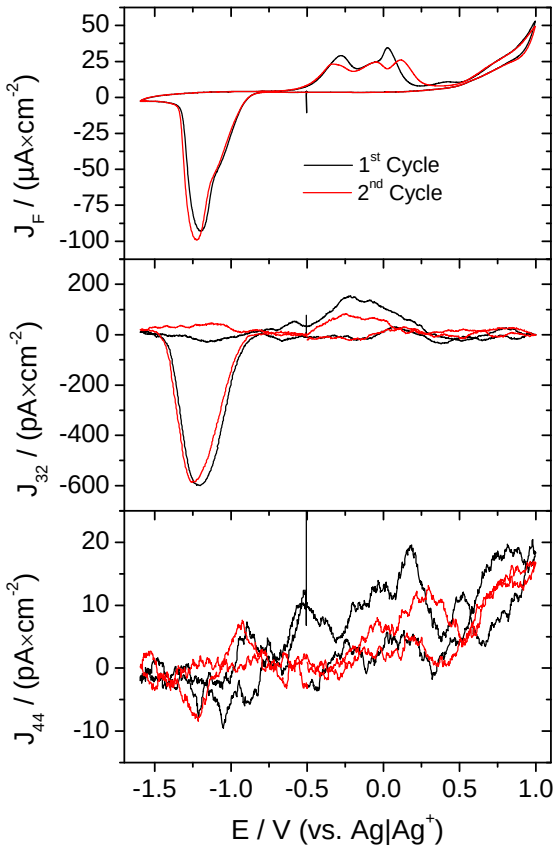

Figure 3: CV (A) and MSCV for mass 32 (B) and mass 44 (C) in an electrolyte of 0.5 M $LiClO_4$ in DMSO purged with a mixture of argon and oxygen (Ar : O_2 = 80 : 20); Sweep rate: 10 mV/s; Flow rate: 5µL/s; Electrode: Au(111) single crystal. Current densities are given with respect to the geometric surface area.

In order to gain a better understanding on why oxygen evolution at a gold electrode is different from that on other electrode materials we repeated the experiment with an Au(111) single crystal. The resulting CVs and MSCVs are shown in Figure 3. Qualitatively the region of oxygen reduction is not different from that obtained at a polycrystalline electrode. The roughness factor of a single crystal is one. Hence, less Li_2O_2 is deposited on the electrode and the electrode is deactivated at lower overpotentials than at the rough electrode. However, the region of oxygen evolution is different from that in Figure 1. In the first anodic sweep at the single crystal two peaks are present. Because of the bad signal to noise level in the MSCV for mass 32 it is not clear whether both peaks are connected to oxygen evolution. After the electrode was polarised to a potential, where roughening occurs, changes appeared in the CV.

In the region of oxygen evolution three peaks appear with the third peak at 0.15 V. Except for the third peak which is much more pronounced the CV for the second sweep at the single crystal resembles that of the rough electrode. The changes observed in the CV in the potential region of oxygen evolution when the surface of the electrode is roughened suggest a strong interaction between the gold surface and the deposited Li_2O_2. This would explain why a portion of the Li_2O_2 appears to be thermodynamically more stable which was already pointed out for the polycrystalline gold electrode. However, more work on that issue is required to ensure the interpretation presented herein.

We consider glassy carbon as a model material for carbon black, which is used to manufacture gas diffusion electrodes in model lithium air batteries. Even though oxygen evolution at glassy carbon proceeds with a low current density (note that only 4.38 nmol/cm^2 of oxygen are evolved from that electrode) the overpotential is low. Thus, glassy carbon has reasonable activity for oxygen evolution. The difference between the onset potential for oxygen reduction and for oxygen evolution amounts only to 0.4 V (Figure 2). Therefore, it seems unlikely that the lack of activity for Li_2O_2 oxidation of the carbon black substrate causes the high charging overpotentials observed in literature[15].

	$n(O_2)_{ORR}$ / (nmol cm^{-2}) (Q_{32} / pC cm^{-2})	$n(O_2)_{OER}$ / (nmol cm^{-2}) (Q_{32} / pC cm^{-2})	$n(O_2)_{OER}$ / $n(O_2)_{ORR}$	RF	$\theta(Li_2O_2)$ / (ML)
Gold (ref.[50])	6.8*) (3738) *)	4.2*) (2311) *)	0.62	10	1.7
Gold (RF~3)	12.2 (11728)	4.9 (4750)	0.41	3	2.0
Gold (RF~1)	21.6 (20830)	4.4 (4286)	0.21	1	1.8
Gold (Au(111))	18.2 (17561)	7.2 (6978)	0.40	1	2.9
Platinum (RF = 5.5)	5.6 (5430)	2.3 (2183)	0.40	5.5	1.0
Platinum (RF = 1.7)	10.3 (9929)	2.8 (2708)	0.27	1.7	1.3
Rhodium	2.8 (2680)	1.5 (1465)	0.55	10.8	0.6
Rh/Se	2.9 (2764)	1.0 (993)	0.36	10.8 (θ_{Se} = 0.72)	0.4
Ruthenium	25.2 (24310)	4.2 (4089)	0.17	1.15	2.0
Glassy Carbon	32.7#) (31501#))	4.4#) (4226#))	0.13		

Table 1: Amounts of reduced and evolved oxygen at various electrode materials, calculated from the ionic charge for mass 32 (Q_{32}). All values are given with respect to the true surface area. From these values the true coulombic efficiency was calculated. From the amount of evolve oxygen the surface coverage of Li_2O_2 in terms of mono layers (ML) deposited on the electrode was determined. *) Values determined from the curves shown in reference[50]; #)With respect to the geometric surface area of 0.283 cm^2

It has been shown several times before that the true coulombic efficiency of oxygen reduction (e.g. the ratio of reduced to evolved oxygen) significantly deviates from 100%[10, 35,

[50]. Table 1 lists the amounts of reduced and evolved oxygen and the corresponding true coulombic efficiency (defined as the ratio of the amount of evolved to reduced oxygen) at the various electrode materials with various roughness factors. At no electrode material the true coulombic efficiency is even close to 100%. In the present study this is to some degree due to convection, that removes superoxide (*vide infra*) from the electrode. Therefore, the corresponding amount of oxygen is not available for oxygen evolution in the anodic sweep. But even with the rhodium electrode where oxygen reduction nearly entirely precedes via the direct electrochemical formation of peroxide the true electrochemical reversibility remains below 60% (*vide infra*). In addition Table 1 lists the surface coverage of lithium peroxide which was calculated from the amount of evolved oxygen. These values show that only very limited amounts of oxygen are deposited on the electrode and that the maximum surface coverage of Li_2O_2 depends on the electrode material. However, we cannot give any explanation at this point why gold and ruthenium allow the formation of 2 ML of Li_2O_2, whereas at platinum only one and at rhodium a submonolayer is deposited.

At all electrode materials under consideration there is a signal in the MSCV for mass 44. This signal is most probably due to CO_2 evolution. With the exception of the experiments done with the glassy carbon electrode there is no other source of carbon except for DMSO. Hence, the evolution of CO_2 is indicative for electrolyte decomposition. McCloskey *et al.* have proposed for DMSO and other solvents that CO_2 evolution is due to a parasitic reaction of Li_2O_2 with the solvent[10]. Although the signal intensity of the ionic current for mass 44 varies with the electrode material - there is hardly any CO_2 evolution at ruthenium and rhodium but a clear signal at the remaining electrode materials - CO_2 is probably not the result of mere electrooxidation of the electrolyte.

The decomposition of the electrolyte consumes a portion of the reduced oxygen. Hence, there is a deviation of the true coulombic efficiency from 100%. Therefore, we consider it important, to look for new electrolytes that are stable against the exposure to peroxide.

Influence of the Electrode Material on Oxygen Reduction

Since the ionic current for mass 32 is proportional to the amount of consumed and evolved oxygen per time and the faradic current is proportional to the conversion rate of oxygen times the number of transferred electrons (z) it is possible to calculate z from the ratio of I_F and I_{32} according to Equation 1.

$$z = \frac{I_F}{I_{32}} \cdot K^* \text{ (eq. 1)}$$

where K* is a calibration constant obtained in a separate experiment. In order to calculate accurate z-values I_F was corrected for the double layer charging by subtracting a straight line. Both, double layer charging and side reactions, would alter the calculated z-value.

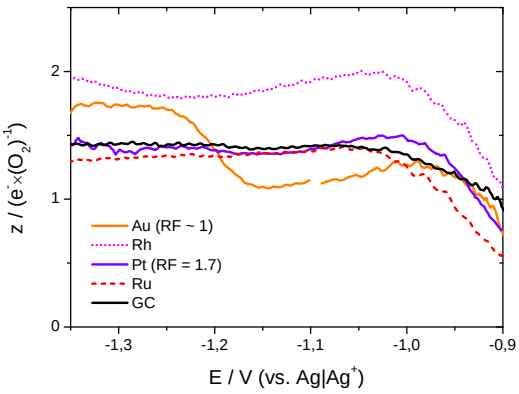

Figure 4: Number of electrons (z) that are transferred per molecule of oxygen in the potential region of oxygen reduction at various electrode materials. Electrolyte: 0.5 M $LiClO_4$ in DMSO; Sweep rate: 10 mV/s; Flow rate: 5µL/s.

Figure 4 shows the number of electrons that are transferred per molecule of oxygen during oxygen reduction at various electrode materials. At a gold electrode z initially has a value of approximately 1 e^-/O_2. From that we conclude that at low overpotetentials superoxide is formed upon oxygen reduction. Although superoxide is instable in the presence of Li^+ and disproportionates to peroxide and oxygen, this reaction is relatively slow, as no appreciable amount of superoxide has disproportionated in the time it takes (approximately 2 seconds) to transport it from the upper compartment of the dual thin layer cell to the lower compartment. (O_2 thus formed leads to a diminution of the amount of consumed O_2 and thus to an increase of z). The long life time of superoxide in DMSO was assigned to the high donor number of 125 kJ/mol[43], enabling the solvent to stabilise Li^+ [7]. At -1.2 V the mechanism of oxygen reduction changes from an indirect pathway to a direct pathway of peroxide formation. This is indicated by the change of the z-value from approximately 1 e^-/O_2 to approximately 2 e^-/O_2. Qualitatively, this is also visible from the shoulder in the CV for the Au-surfaces in Figure 1 and Figure 3, which does not appear in the MSCVs.

Comparison of the z-values observed at the gold electrode to the z-values observed at other electrode materials under review reveals that such a change from the indirect to the direct pathway of peroxide formation proceeds only at gold. The difference to the rhodium electrode is most striking. At this electrode oxygen reduction proceeds via the transfer of 2 e^-/O_2 throughout the whole potential region of oxygen reduction, whereas the indirect pathway via superoxide formation is of little significance.

At platinum, ruthenium and glassy carbon electrodes the transfer of about 1.5 e^-/O_2 is observed during oxygen reduction. It seems that at these electrodes both pathways of peroxide formation, the direct and the indirect, are in place at all potentials, so that roughly half the oxygen is reduced to superoxide and the other half forms peroxide.

Equation 1 from which the z-values in Figure 4 were calculated only holds when there is no electrochemical side reaction occurring in the potential region of oxygen reduction. In order to rule out any such side reaction CVs were recorded in argon saturated electrolyte of 0.5 M $LiClO_4$ in DMSO at all electrode materials under review. No such side reaction was observed. However, especially at rhodium electrodes a surface oxide might form in an oxygen containing electrolyte, whereas this reaction does not necessarily occur in an argon saturated electrolyte. Pseudocapacitances due to the reduction of such a surface oxide would significantly alter the observed z-values. For that reason oxygen reduction was also examined at a selenium decorated polycrystalline rhodium electrode. The corresponding CVs and MSCVs are shown in Figure 1S. It was shown previously that transition metal surfaces

modified with chalcogenides have enhanced stability and are less likely to form a surface oxide[59-61]. Therefore, in the potential region of oxygen reduction no contribution to the current due to pseudo capacities is expected, when a selenium modified rhodium is used as a working electrode.

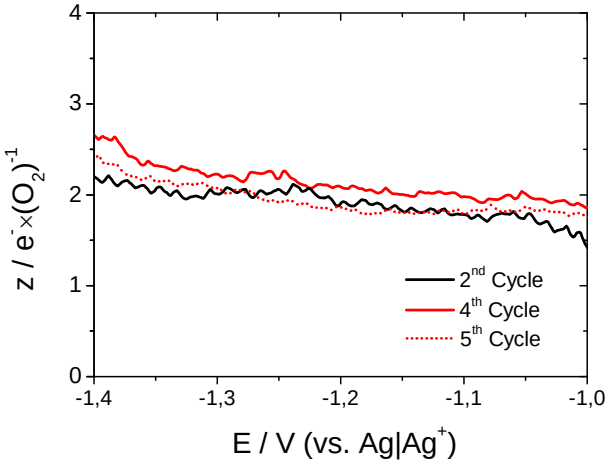

Figure 5: z-values during oxygen reduction obtained at an rhodium electrode modified with approximately 0.72 ML of Se. The values were calculated according to equation 1 from the curves shown in Figure 1S. Black: before Se stripping; red: after Se-stripping.

Figure 5 displays the z-values obtained at a Se-modified rhodium electrode as a function of potential. There are little differences before (2nd and 4th cycle) and after (5th cycle) Se stripping. In Figure 5 oxygen reduction proceeds via the transfer of 2 e^-/O_2 as already observed at the unmodified rhodium electrode. Since pseudo capacities due to the reduction of a surface oxide are unlikely to contribute to the current observed in the potential region of oxygen reduction at a selenium modified electrode, it is also unlikely that the observed z-values are distorted by any side reaction.

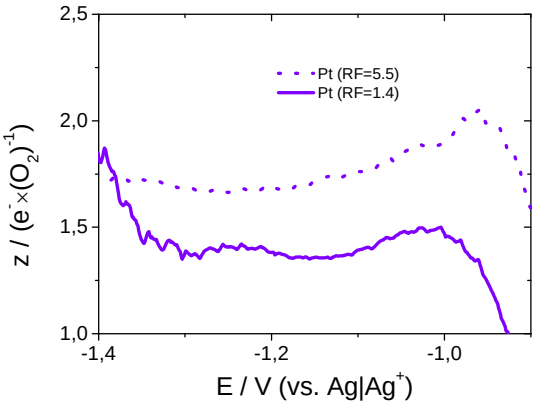

Figure 6: Number of electrons (z) that are transferred per molecule of oxygen in the potential region of oxygen reduction at a platinum electrode. Dotted: With a roughness factor of 5.5; Solid: With a roughness factor of 1.7; Electrolyte: 0.5 M $LiClO_4$ in DMSO; Sweep rate: 10 mV/s; Flow rate: 5µL/s.

In aqueous electrolytes platinum is the most active material for the oxygen reduction reaction among all metals. In addition oxygen reduction at Pt electrodes results nearly exclusively in the formation of water, when the reaction is conducted in acid electrolytes[62, 63]. For that reason it seems strange that oxygen reduction in DMSO based electrolytes does not

proceed exclusively via the direct pathway of peroxide formation, as observed at the rhodium electrode.

Figure 6 compares the z-values observed at a Pt-electrode with a roughness factor of 1.7 (already included in Figure 4) with those observed at a Pt-electrode with a roughness factor of 5.5. From Figure 6 it becomes clear that the roughness factor has an influence on the observed z-values. At the rough Pt-Electrode more electrons are transferred per oxygen than at the smooth electrode throughout the entire potential region of oxygen reduction. The difference is most pronounced in the potential range between -0.9 V and -1.0 V, where at both electrodes a peak appears. The increased portion of oxygen that is reduced to peroxide at the rough electrode as compared to the smooth electrode is in accordance with the increased coloumbic efficiency (*c.f.* Table 1).

This peak is not very distinct at the smooth electrode but at the rough electrode z increases to 2 e^-/O_2 in a small potential range. During oxygen reduction Li_2O_2 is deposited on the surface of the electrode. Increasing the roughness changes the ratio of the portion of the surface that is not covered with Li_2O_2 to the portion of the surface that is blocked already. Therefore, a larger portion of the surface of the rough electrode is still not covered by Li_2O_2 than of the smooth electrode at any given potential.

The fact that more electrons per oxygen are transferred when the electrode is relatively free of any deposit (low overpotentials and high roughness) than when it is covered to a large degree by Li_2O_2 (large overpotentials low roughness) points to a poisoning of the electrode as Li_2O_2 precipitates. The impact of a deposit on the z-value is not simply due to a blocking of the electrode (although blocking of the electrode also occurs). In this case less oxygen would be reduced and the reduction current would drop correspondingly, hence, leaving the observed z-value unaffected. However, deposition of Li_2O_2 on a Pt-Electrode reduces the ability of the latter to reduce oxygen via the direct pathway of peroxyde formation, while the ability to form superoxide is maintained.

As shown above, deposition of 1 ML Li_2O_2 (here a ML is defined as a unit of Li_2O_2 per surface atom) blocks the Pt-electrode entirely. Hence, there is no oxygen reduction taking place at those parts of the surface that are covered by Li_2O_2. Consequently the increasing degree of superoxide formation with an increasing degree of surface coverage is not due to a change of the reaction side.

The catalytic performance of an electrode may be altered by an adlayer in three different ways: By a bifunctional mechanism, by a ligand-effect or by a geometric effect[64]. It is rather unlikely that an insulator exerts a ligand-effect. A bifunctional mechanism is expected when two intermediates adsorbed at the surface of the electrode react. Such a mechanism is hard to imagine as intermediates other than reduced oxygen species are not expected to be of any importance for the oxygen reduction reaction in organic electrolytes. However, Li_2O_2 might exert a geometric effect, when more than one surface atom of the Pt-electrode is required in order to form peroxide via the direct pathway.

Working in aqueous electrolytes, Adžić and Wang showed that oxygen reduction at Pt(111) electrodes is inhibited by Ag-Adatoms [65]. From that they concluded that oxygen adsorption at bridge sites precedes oxygen reduction. Furthermore they concluded that prior to the $4e^-$-reduction the oxygen-oxygen bond is disrupted. Similarly in organic electrolytes the $2e^-$-reduction at polycrystalline platinum electrodes could require the weakening of the oxygen-oxygen bond by adsorption in a bridge position.

From a fundamental point of view it is interesting to note that oxygen reduction does not proceed via a $4e^-$-process at platinum electrodes in DMSO based electrolytes: There is abundant experimental proof that oxygen is reduced to water when aqueous electrolytes are employed [62, 63]. Indeed, for aqueous systems the cleavage of the O-O bond is expected at surfaces that strongly bind oxygen, such as platinum, while a $2e^-$-process is observed at

weakly oxygen-binding surfaces such as Au(111) [66] and on Pt-surfaces partially blocked [65]. Also, McCloskey *et al*. observed the that increasing amounts of CO_2 were evolved when recharging a Li-O_2 battery that employed a DME based electrolyte, when instead of a gold or carbon electrode a platinum containing electrode was used [67]. The formation of CO_2 involves at some point the cleavage of the O-O-bond. However, it is not clear whether cleavage of the bond occurs during discharge or charge (*e.g*. the cleavage could occur during oxidation of an organic peroxide that favourably forms at platinum electrodes during oxygen reduction).

Notwithstanding this, we do not observe the cleavage of the O-O-bond (except for the evolution of minor quantities of CO_2) regardless of the electrode material. However, oxygen reduction in DMSO base electrolytes shows some parallels to oxygen reduction in aqueous solution if the direct pathway of peroxide formation is considered the organic analogue of the $4e^-$-process. Platinum catalyses in aqueous electrolytes predominantly the formation of water[62, 63], but shows sensitivity towards adlayers and impurities, which tilt product distribution towards hydrogen peroxide formation[65, 68-70]. Similarly oxygen reduction in DMSO based electrolytes at platinum proceeds initially by the direct pathway of peroxide formation. However, as the electrode is increasingly covered with Li_2O_2 the indirect pathway of peroxide formation gains importance. At gold electrodes in aqueous solution hydrogenperoxide is the dominant product of oxygen reduction[71, 72], whereas only superoxide is formed at low overpotentials in DMSO based electrolytes. Therefore, we wonder whether the same mechanisms and parameters that sustain the $4e^-$-process in aqueous electrolytes are also at work in order to foster the direct pathway of peroxide formation.

Irrespective of the detailed mechanism of oxygen reduction at platinum, it is clear that the nature of the surface plays a crucial part in oxygen reduction. This is not only clear from what we believe to be a geometric effect of the Li_2O_2 deposit on the platinum electrode, that tilts the mechanism of oxygen reduction away from the direct to the indirect pathway. Figure 4 shows that there is a more general influence of the electrode material: While at gold and at low overpotentials oxygen is reduced to superoxide, peroxide is formed at rhodium.

It is rather unexpected to observe an electrocatalytic effect of the electrode material on the oxygen reduction reaction in organic electrolytes. The oxygen reduction reaction in DMSO proceeds without the disruption of the oxygen-oxygen bond and very close to the thermodynamic potential of Li_2O_2-formation (Onset of oxygen reduction: -0.88 V; thermodynamic potential of peroxide formation versus Ag/Ag^+: -0.79 V[7, 51]). Therefore, we expected the oxygen reduction reaction to be an outer sphere reaction. At least for the direct pathway of peroxide formation this is clearly not the case, where the influence of the electrode material suggests an inner sphere reaction.

Our finding of an electrocatalytic effect of the electrode material is supported by the findings of Lu *et al*. [22]. These authors found a volcano like behaviour, when they plotted the potential, at which a certain current density was observed, against the adsorption enthalpy of oxygen at the used electrode material.

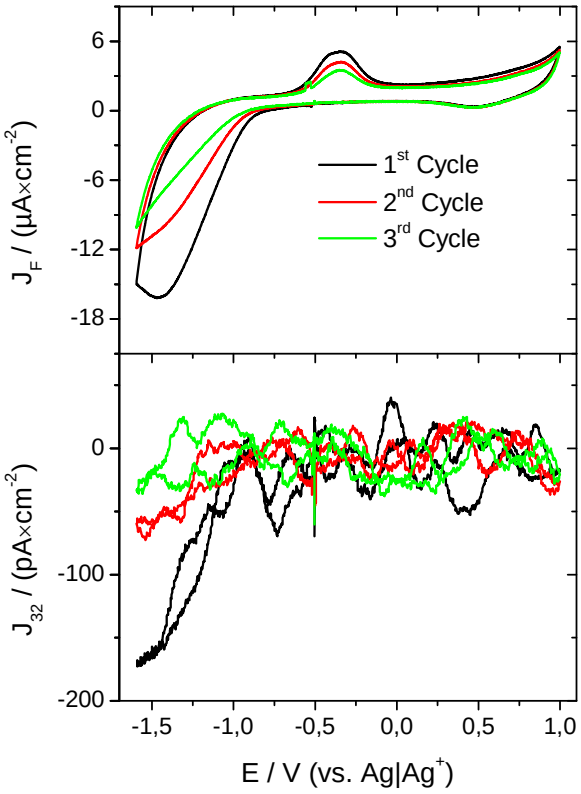

Figure 7: CV (A) and MSCV for mass 32 (B) in an electrolyte of 0.5 M $LiClO_4$ in DMSO purged with a mixture of argon and oxygen (Ar : O_2 = 80 : 20) at a BDD electrode with H-terminated surface (BDD_{red}); Sweep rate: 10 mV/s; Flow rate: 5µL/s. Current densities are given with respect to the geometric surface area.

Figure 7 shows the CV and MSCVs for mass 32 in an electrolyte of 0.5 M $LiClO_4$ in DMSO at a hydrogen terminated BDD-electrodes. The current density at BDD_{red} reduces from cycle to cycle while the CV at BDD_{ox} (Figure S2) remains relatively constant and resembles that obtained in the third cycle at BDD_{red}. This observation might be due to the oxidation of the BDD_{red}-electrode at high potentials. Both at BDD_{red} and BDD_{ox} oxygen reduction takes place at -0.9 V at the same potential as with the other electrode materials. However, the observed current densities at both electrodes are much lower than at all the other electrode materials under review.

It was shown for acid solutions that, contrary to oxygen evolution and other oxidation reaction which proceed via OH radicals [73, 74], oxygen reduction proceeds at functional groups such as quinons, formed from sp^2-carbon impurities in the surface of the BDD-electrode upon oxidation, at potentials significantly larger than at the diamond surface[75]. The nature of these functional groups and their capacity to catalyse electrochemical reactions depends on the way the electrode is terminated[75, 76]. Both, the overall low current density observed at the BDD-electrodes as compared to other electrode materials as well as its sensitivity to the termination mode of the electrode (terminated by hydrogen or oxygen *c. f.* Figure S2), suggest that the oxygen reduction observed in Figure 7 does not proceed at the diamond surface itself but at functional groups on the BDD surface, as was previously observed in aqueous solutions.

Reactions that involve the formation of adsorbed intermediates at other electrode materials proceed at BDD electrodes only at rather large overpotenials. Outer sphere reactions on the other hand are highly reversible at BDD electrodes. The absence of oxygen reduction at the BDD-electrode suggests that also superoxide formation is an inner sphere reaction that requires specific adsorption of O_2 at the surface of the electrode. In this context it is

noteworthy that 1 ML of Li_2O_2 on platinum and 2 ML on gold are sufficient to deactivate the electrode entirely. If oxygen reduction was an outer sphere reaction, tunnelling of electrons through the Li_2O_2-layer would allow the continuous formation of superoxide.

Influence of Cations on Oxygen Reduction

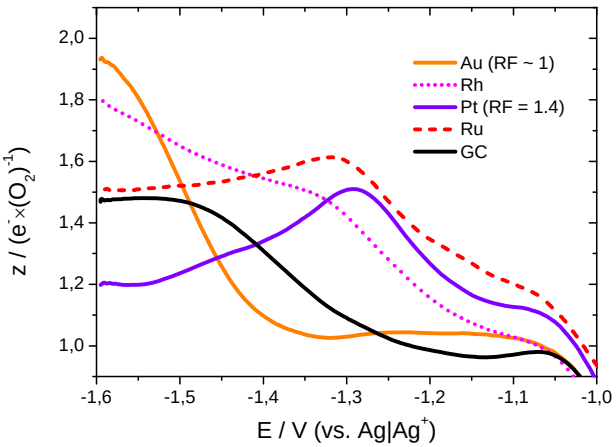

Figure 8: Number of electrons (z) that are transferred per molecule of oxygen in the potential region of oxygen reduction. Black/solid: At glassy carbon; Red/dashed: At ruthenium; Purple/solid: At platinum; Magneta/dotted: At rhodium; Orange/solid: At gold. Electrolyte: 0.5 M $NaClO_4$ in DMSO; Sweep rate: 10 mV/s; Flow rate: 5µL/s.

An inner sphere reaction suggests that the structure of the electrochemical double layer at the interface between the electrode and the electrolyte exerts an effect on the mechanism of oxygen reduction. Different conducting salts or additives should alter the structure of the double layer and consequently could influence the mechanism of oxygen reduction.

Figure 8 shows the z-values for the oxygen reduction reaction as a function of potential observed in an electrolyte of 0.5 M $NaClO_4$ in DMSO. The values in Figure 8 were obtained in the same way as those displayed in Figure 4. As an example Figure 9 shows the corresponding CVs and MSCVs obtained at platinum and gold. The CV- and MSCV-data at rhodium, ruthenium and glassy carbon are available in the supporting information (Figures S3 – S5).

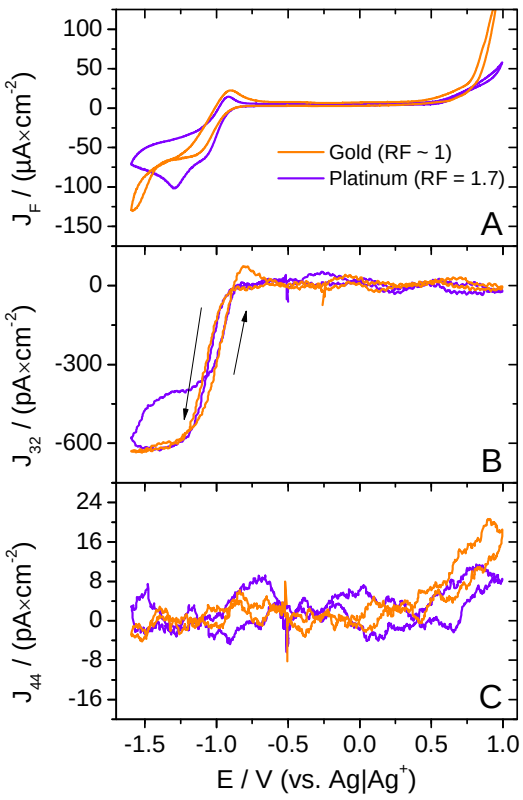

Figure 9: CV (A) and MSCV for mass 32 (B) and mass 44 (C) in an electrolyte of 0.5 M $NaClO_4$ in DMSO purged with a mixture of argon and oxygen (Ar : O_2 = 80 : 20); Sweep rate: 10 mV/s; Flow rate: 5µL/s; orange: At a gold electrode (RF ~3); Purple: At a platinum electrode (RF = 5.5). Current densities are given with respect to the geometric surface area.

In Figure 8 the most pronounced difference to Figure 4 occurs at the gold electrode. In both, lithium and sodium containing electrolytes, the z-value increases from 1 e^-/O_2 to 2 e^-/O_2 as the potential decreases. However, this increase is delayed by 200 mV from -1.2 V in the lithium-containing electrolyte to -1.4 V in the sodium-containing electrolyte. Furthermore the z-value observed at all electrode materials starts out close to 1 e^-/O_2 and then increases as the overpotential increases. In Figure 4 only gold shows this behaviour. At ruthenium and more pronounced at platinum the z-value passes through a maximum. This is probably due to the same effect as observed in Figure 6. Deposits on the electrode surface inhibit the ability of the electrode to sustain the direct pathway of peroxide formation.

From the comparison of the z-values in Figure 8 to those in Figure 4 it becomes clear that the cation exerts an effect on the oxygen reduction. Since the thermodynamic potential of Na_2O_2-formation is at -0.97 V ($E_0(Li_2O_2)$ = -0.79 V versus Ag/Ag [7, 51]) and that of NaO_2-formation at -1.03 V versus Ag/Ag^{+}[42, 51] the observed effect is of kinetic nature. Not only sodium but also other cations alter the potential at which the direct pathway of peroxide formation is observed. The charge density of the cation seems to be the crucial parameter. This is shown by Figure 10, where the half wave potential of peroxide formation at a gold electrode is plotted against the charge density of the cation. We cannot give any explanation for the linear dependency observed in Figure 10. However, it was shown by Si and Gewirth[77] that the addition of nitric acid changes the structure of DMSO adsorbed at the non-polarised Au(111) surface. An altered structure (due to a change of the conducting salt) at the interface between the electrode and the electrolyte should have an influence on an inner sphere reaction.

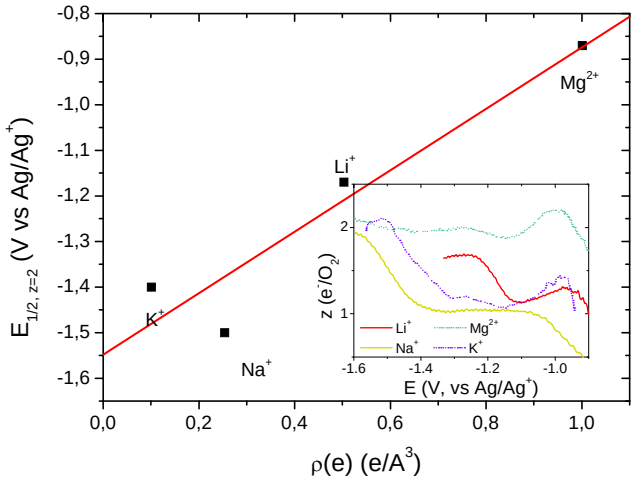

Figure 10: Plot of the half wave potential at which the transfer of 2 electrons per molecule of oxygen is observed at gold, against the charge density ρ(e) of the cation of the conducting salt. Electrolyte: 0.5 M of the respective perchlorate in DMSO (0.4 M $Mg(ClO_4)_2$ in DMSO); Sweep rate: 10 mV/s; Flow rate: 5µL/s. The CV and MSCV of the potassium and magnesium containing electrolyte are available in the supporting information (Figures S14 and S15).

Alternatively, the relationship between half wave potential of peroxide formation and charge density of the cation might originate from the mechanism of oxygen reduction. It is hard to imagine that peroxide formation proceeds via two subsequent single electron transfers (SET), thus, creating a highly charged O_2^{2-}. It is more likely that coordination of the cation to adsorbed superoxide is required in order to facilitate the second SET.

It is clear that coordination of a cation with larger charge density would polarise adsorbed superoxide more effectively. Hence, a cation with large charge density could facilitate the second SET at lower overpotentials.

The Effect of Water on Oxygen Reduction

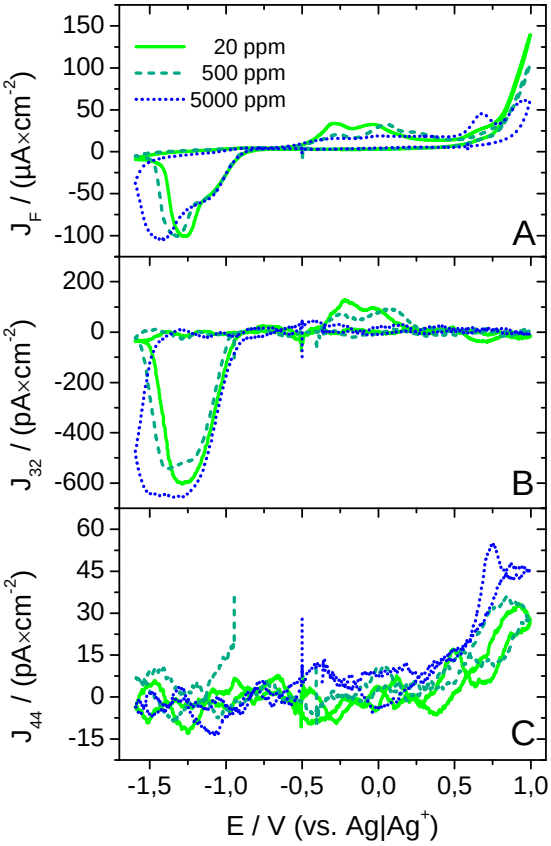

Figure 11: CV (A) and MSCV for mass 32 (B) and mass 44 (C) in an electrolyte of 0.5 M $LiClO_4$ in DMSO with various water contents and purged with a mixture of argon and oxygen (Ar : O_2 = 80 : 20); Sweep rate: 10 mV/s; Flow rate: 5µL/s; Electrode: Au(pc); solid: 20 ppm water (absolute); dashed: 500 ppm water (added); dotted: 5000 ppm water (added). Current densities are given with respect to the geometric surface area.

Metal air batteries are supposed to work under ambient conditions with oxygen supplied by the air. Hence, humidity is always present and might affect the charge and discharge of the battery. Therefore, we investigated the effect of the water content on oxygen reduction reaction. Figure 11 shows the CV and MSCV for mass 32 and 44 obtained in an electrolyte of 0.5 M $LiClO_4$ in DMSO with various water contents at a gold electrode. In addition, Figure 12 shows the z-values calculated from the CV and MSCV data shown in Figure 11. The CVs and MSCVs as well as the calculated z-values that were obtained with various water contents in the electrolyte at the remaining electrodes are available in the supporting information (Figures S6 - S13).

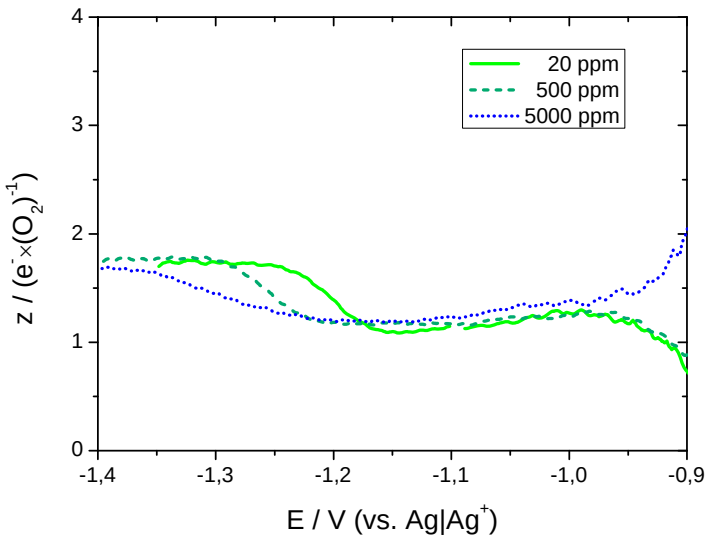

Figure 12: Number of electrons (z) that are transferred per molecule of oxygen in the potential region of oxygen reduction at a polycrystalline gold electrode in an electrolyte of 0.5 M $LiClO_4$ in DMSO with various water contents. Solid: 20 ppm water (absolute); dashed: 500 ppm water (added); dotted: 5000 ppm water (added); Sweep rate: 10 mV/s; Flow rate: 5µL/s.

From the z-values presented in Figure 12 it is clear that the presence of water inhibits the ability of the gold electrode to form peroxide. In this respect gold is unique among the electrode materials under review as the water content has no effect on the z-values obtained at the other electrodes. Since only at gold a step in the z-value is observed when a lithium-containing electrolyte is employed, it is not surprising that the water effect is restricted to this electrode material. The direct pathway of peroxide formation is an inner sphere reaction (as derived from the results presented in Figure 4) suggesting that also water exerts an effect on the double layer structure. However, it is less clear than in the case of the cation that water even participates in the formation of the double layer. From the ESI results presented in Figure 13 we can at least rule out any effect of water on the solvation sphere of the cation:

In Figure 13A the ESI spectrum of 1 mM LiTfO in DMSO is shown. A peak appears at mass 163 and another at 241 corresponding to $[Li(DMSO)_2]^+$ and $[Li(DMSO)_3]^+$, respectively. From that we take that Lithium is solvated in DMSO by two to three solvent molecules. When the DMSO based electrolyte is mixed with another electrolyte consisting of a 1:1 mixture of methanol and water plus 1% acetic acid the spectrum does not change in Figure 13B. There is no peak that corresponds to the substitution of DMSO by water or methanol in the solvation sphere of lithium. Hence, the solvation shell of Li^+ remains unaltered when water is added to the electrolyte. The effect of water on the oxygen reduction reaction as described above does not stem from a solvation effect of lithium.

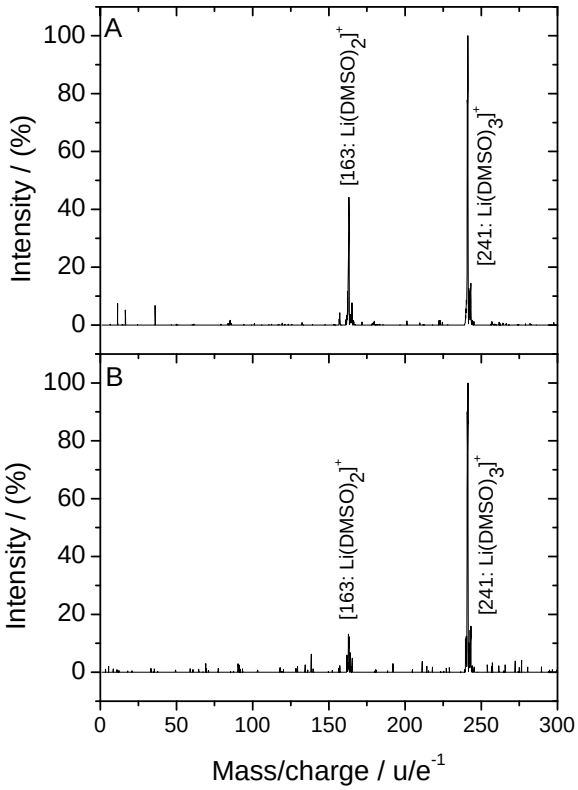

Figure 13: ESI spectrum of A: 1 mM LiTfO in DMSO and B: 50% 1 mM LiTfO in DMSO and 50% of a 1:1 mixture of water and methanol containing 1% CH_3COOH.

It was recently found that water favours the formation of large NaO_2 crystallites upon discharge of sodium-oxygen batteries[36]. The authors of that paper considered water as a proton phase transfer catalyst, with water donating a proton to NaO_2 in order to solubilize it as HO_2. In that view HO_2 can diffuse to certain nucleation sites and deposit as NaO_2, thus forming larger particles. Also for the formation of toroide shaped Li_2O_2 particles in lithium-oxygen batteries a similar mechanism was proposed, that is driven by a better solubility of LiO_2 in water containing electrolytes [17]. However, we do not believe that acidity of water is a viable explanation for the effect observed in Figure 12. Water has a pK_a value of 31.2 in DMSO, whereas DMSO in DMSO has a pK_a value of 35[78]. With a water concentration of 500 ppm (aproximatly 25 mmol/l), at which a clear effect of water is observed already, and a DMSO concentration of approximately 14 mol/l the concentration of protons in the electrolyte is increased 10 fold at best. Considering that coordination of Li^+ to DMSO probably enhances its acidity, the relative increase of the proton concentration due to water is likely to be lower. However, one order of magnitude in the proton concentration might make the difference whether an acid-base reaction occurs or not. But even if the concentration of protons was sufficient to influence the mechanism of oxygen reduction we would rather expect protons, with their high charge density, to favour the direct pathway of peroxide formation (*c.f.* Figure 10).

Others, working in the field of Li-O_2 batteries, have considered the formation of toroid shaped Li_2O_2 particles of a mechanism, that is driven by an enhanced solubility of LiO_2, in the presence of water[17]. Indeed, it has been found that the acceptor number (AN) of a solvent will largely affect the solubility of superoxide [79]. Since water has a much larger acceptor number (AN = 229 kJ/mol [80]) than DMSO (AN = 81 kJ/mol [80]), the enhanced solubility of water seems a viable explanation for the delayed peroxide formation with increasing water content.

In Figure 11C the amount of evolved CO_2 increases as the water content in the electrolyte is increased. The effect is small, but is present at all electrode materials. It was reported that CO_2 is only formed in this electrolyte after oxygen reduction[10]. Therefore, the evolution of CO_2 in the anodic sweep is the result of oxidation of decomposition products formed during oxygen reduction in the preceding cathodic sweep. However, it is not clear whether enhanced CO_2 evolution is due to the facilitated electrolyte decomposition during oxygen reduction or due to the facilitated oxidation of these decomposition products in the presence of water.

Conclusions

By correlating the consumed amounts of oxygen as obtained by DEMS with the faradaic current, the number of electrons transferred per molecule of oxygen during oxygen reduction was calculated as a function of potential. Distinctively different behaviors were observed at different electrode materials: Oxygen reduction in a lithium containing electrolyte at rhodium electrodes proceeds via the direct electrochemical formation of peroxide, while at platinum, ruthenium and glassy carbon electrodes both the direct and the indirect formation of peroxide take place in parallel. Only at gold electrodes a transition from the indirect to the direct pathway was observed when the applied overpotential was increased. Such a transition at different overpotentials was observed with all electrode materials when a sodium containing electrolyte was used. This shows that the electrode material exerts a catalytic effect, and that peroxide formation is not an outersphere reaction. Based on differences observed in the electron number, when platinum electrodes with different roughness factors were employed, it was proposed that the Li_2O_2-deposit exerts a geometric effect.

The required overpotential to observe the transition from the indirect to the direct pathway of peroxide formation at gold electrodes in lithium containing electrolytes is sensitive to the water content in the electrolyte. With increasing water content also the required overpotential increases. This effect is not due to an altered solvation shell of Li^+ in the presence of water, as it is always coordinated by two or three molecules of DMSO, irrespective of the presence of water. Therefore, it was proposed that the effect is due to an alteration of the structure of the double layer in front of the electrode.

Comparing the current densities due to oxygen evolution at platinum and gold electrodes with similar Li_2O_2 coverages showed enhanced kinetics at the platinum electrode. This also suggests a catalytic effect for oxygen evolution. In the CV at gold single crystals differences to polycrystalline gold were observed in the region of oxygen evolution, suggesting sensitivity to certain surface sites.

Acknowledgement

The authors acknowledge the Federal Ministry of Education and Research for funding this work. This work is part of the “LuLi – Strom aus Luft und Li” project (FKZ:03X4624A).

REFERENCES

1 K. M. Abraham and Z. Jiang, *J. Electrochem. Soc.*, 1996, 143, 1-5.
2 A. Kraytsberg and Y. Ein-Eli, *Journal of Power Sources*, 2011, 196, 886-893.
3 J. Christensen, P. Albertus, R. S. Sanchez-Carrera, T. Lohmann, B. Kozinsky, R. Liedtke, J. Ahmed and A. Kojic, *J. Electrochem. Soc.*, 2012, 159, R1-R30.
4 J. Hou, M. Yang, M. W. Ellis, R. B. Moore and B. Yi, *Physical Chemistry Chemical Physics*, 2012, 14, 13487-13501.
5 D. Capsoni, M. Bini, S. Ferrari, E. Quartarone and P. Mustarelli, *Journal of Power Sources*, 2012, 220, 253-263.

6 Z. Peng, S. A. Freunberger, Y. Chen and P. G. Bruce, *Science*, 2012, 337, 563-566.
7 C. O. Laoire, S. Mukerjee, K. M. Abraham, E. J. Plichta and M. A. Hendrickson, *J. Phys. Chem. C*, 2010, 114, 9178-9186.
8 D. Xu, Z.-l. Wang, J.-j. Xu, L.-l. Zhang, L.-m. Wang and X.-b. Zhang, *Chemical Communications*, 2012, 48, 11674-11676.
9 W. Xu, J. Hu, M. H. Engelhard, S. A. Towne, J. S. Hardy, J. Xiao, J. Feng, M. Y. Hu, J. Zhang, F. Ding, M. E. Gross and J.-G. Zhang, *Journal of Power Sources*, 2012, 215, 240-247.
10 B. D. McCloskey, D. S. Bethune, R. M. Shelby, T. Mori, R. Scheffler, A. Speidel, M. Sherwood and A. C. Luntz, *The Journal of Physical Chemistry Letters*, 2012, 3, 3043-3047.
11 M. W. Chase, Jr., *Journal of Physical and Chemical Reference Data*, 1998, Monograph 9, 1-1951.
12 J. D. Cox, D. D. Wagman and V. A. Medvedev, *Hemisphere Publishing Corp., New York*, 1989.
13 B. D. Adams, C. Radtke, R. Black, M. L. Trudeau, K. Zaghib and L. F. Nazar, *Energy & Environmental Science*, 2013, 6, 1772-1778.
14 R. R. Mitchell, B. M. Gallant, Y. Shao-Horn and C. V. Thompson, *The Journal of Physical Chemistry Letters*, 2013, 4, 1060-1064.
15 A. C. Luntz and B. D. McCloskey, *Chemical Reviews*, 2014, 114, 11721-11750.
16 V. Viswanathan, K. S. Thygesen, J. S. Hummelshoj, J. K. Norskov, G. Girishkumar, B. D. McCloskey and A. C. Luntz, *J. Chem. Phys.*, 2011, 135, 10.
17 N. B. Aetukuri, B. D. McCloskey, J. M. García, L. E. Krupp, V. Viswanathan and A. C. Luntz, *Nat Chem*, 2014, 7, 50-56.
18 K. U. Schwenke, M. Metzger, T. Restle, M. Piana and H. A. Gasteiger, *J. Electrochem. Soc.*, 2015, 162, A573-A584.
19 M. Safari, B. D. Adams and L. F. Nazar, *The Journal of Physical Chemistry Letters*, 2014, 5, 3486-3491.
20 A. K. Thapa and T. Ishihara, *Journal of Power Sources*, 2011, 196, 7016-7020.
21 A. K. Thapa, Y. Hidaka, H. Hagiwara, S. Ida and T. Ishihara, *J. Electrochem. Soc.*, 2011, 158, A1483-A1489.
22 Y.-C. Lu, H. A. Gasteiger and Y. Shao-Horn, *Journal of the American Chemical Society*, 2011, 133, 19048-19051.
23 S. A. Freunberger, Y. Chen, N. E. Drewett, L. J. Hardwick, F. Barde and P. G. Bruce, *Angewandte Chemie-International Edition*, 2011, 50, 8609-8613.
24 S. A. Freunberger, Y. Chen, Z. Peng, J. M. Griffin, L. J. Hardwick, F. Barde, P. Novak and P. G. Bruce, *Journal of the American Chemical Society*, 2011, 133, 8040-8047.
25 X. Ren, S. S. Zhang, D. T. Tran and J. Read, *Journal of Materials Chemistry*, 2011, 21, 10118-10125.
26 M. Marinaro, P. Balasubramanian, E. Gucciardi, S. Theil, L. Jörissen and M. Wohlfahrt-Mehrens, *SusChemSus*, 2015, accepted.
27 M. Marinaro, U. Riek, S. K. Eswara Moorthy, J. Bernhard, U. Kaiser, M. Wohlfahrt-Mehrens and L. Jörissen, *Electrochemistry Communications*, 2013, 37, 53-56.
28 C. O. Laoire, S. Mukerjee, K. M. Abraham, E. J. Plichta and M. A. Hendrickson, *J. Phys. Chem. C*, 2009, 113 20127-20134.
29 W. Torres, N. Mozhzhukhina, A. Y. Tesio and E. J. Calvo, *J. Electrochem. Soc.*, 2014, 161, A2204-A2209.
30 W. R. Torres, A. Y. Tesio and E. J. Calvo, *Electrochemistry Communications*, 49, 38-41.
31 M. J. Trahan, S. Mukerjee, E. J. Plichta, M. A. Hendrickson and K. M. Abraham, *J. Electrochem. Soc.*, 2013, 160, A259-A267.
32 D. Sharon, V. Etacheri, A. Garsuch, M. Afri, A. A. Frimer and D. Aurbach, *The Journal of Physical Chemistry Letters*, 2012, 4, 127-131.
33 N. Mozhzhukhina, L. P. MÃ©ndez De Leo and E. J. Calvo, *The Journal of Physical Chemistry C*, 2013, 117, 18375-18380.
34 E. J. Calvo and N. Mozhzhukhina, *Electrochemistry Communications*, 2013, 31, 56-58.
35 B. D. McCloskey, D. S. Bethune, R. M. Shelby, G. Girishkumar and A. C. Luntz, *J. Phys. Chem. Lett.*, 2011, 2, 1161-1166.
36 C. Xia, R. Black, R. Fernandes, B. Adams and L. F. Nazar, *Nat Chem*, 2015, 7, 496-501.
37 L. Andrews, *The Journal of Chemical Physics*, 1969, 50, 4288-4299.
38 W. Liu, Q. Sun, Y. Yang, J.-Y. Xie and Z.-W. Fu, *Chemical Communications*, 2013, 49, 1951-1953.
39 Q. Sun, Y. Yang and Z.-W. Fu, *Electrochemistry Communications*, 2012, 16, 22-25.
40 J. Kim, H.-D. Lim, H. Gwon and K. Kang, *Physical Chemistry Chemical Physics*, 2013, 15, 3623-3629.

41 P. Hartmann, C. L. Bender, M. Vračar, A. K. Dürr, A. Garsuch, J. Janek and P. Adelhelm, *Nat Mater*, 2013, 12, 228-232.
42 C. L. Bender, P. Hartmann, M. Vračar, P. Adelhelm and J. Janek, *Advanced Energy Materials*, 2014, 4, n/a-n/a.
43 V. Gutmann, *Coordination Chemistry Reviews*, 1976, 18, 225-255.
44 R. Cao, E. D. Walter, W. Xu, E. N. Nasybulin, P. Bhattacharya, M. E. Bowden, M. H. Engelhard and J.-G. Zhang, *ChemSusChem*, 2014, 7, 2436-2440.
45 A. A. Abd-El-Latif and H. Baltruschat, in *Encyclopedia of Applied Electrochemistry*, ed. G. Kreysa, K.-i. Ota and R. Savinell, Springer New York Dordrecht Heidelberg London, 2014, pp. 507 - 516.
46 A. A. Abd-El-Latif, C. J. Bondue, S. Ernst, M. Hegemann, J. K. Kaul, M. Khodayari, E. Mostafa, A. Stefanova and H. Baltruschat, *Trends in Analytical Chemistry*, 2015, 70, 4-13.
47 H. Baltruschat, in *Interfacial Electrochemistry*, ed. A. Wieckowski, Marcel Dekker, Inc., New York, Basel, 1999, pp. 577 - 597.
48 H. Baltruschat, *Journal of the American Society for Mass Spectrometry*, 2004, 15, 1693-1706.
49 H. Baltruschat, R. Bussar, S. Ernst and F. Hernandez-Ramirez, in *In-situ Spectroscopic Studies of Adsorption at the Electrode and Electrocatalysis*, ed. S.-G. Sun, P. A. Christensen and A. Wieckowski, Elsevier, Amsterdam, 2007, pp. 471 - 537.
50 C. J. Bondue, A. A. Abd-El-Latif, P. Hegemann and H. Baltruschat, *J. Electrochem. Soc.*, 2014, 162, A479-A487.
51 G. Gritzner, *Journal of Molecular Liquids*, 2010, 156, 103-108.
52 S. Trasatti and O. A. Petrii, *Pure Appl. Chem.*, 1991, 63, 711-734.
53 S. Gilman, *The Journal of Physical Chemistry*, 1967, 71, 4330-4338.
54 T. Nagel, N. Bogolowski and H. Baltruschat, *J. Appl. Electrochem.*, 2006, 36, 1297-1306.
55 J. Clavilier, D. Armand, S. G. Sun and M. Petit, *J. Electroanal. Chem.*, 1986, 205, 267-277.
56 S. Iqbal, C. Bondü and H. Baltruschat, *The Journal of Physical Chemistry C*, 2015, 119, 20515-20523.
57 M. C. Granger, M. Witek, J. Xu, J. Wang, M. Hupert, A. Hanks, M. D. Koppang, J. E. Butler, G. Lucazeau, M. Mermoux, J. W. Strojek and G. M. Swain, *Analytical Chemistry*, 2000, 72, 3793-3804.
58 P. Albertus, G. Girishkumar, B. McCloskey, R. S. Sanchez-Carrera, B. Kozinsky, J. Christensen and A. C. Luntz, *J. Electrochem. Soc.*, 2011, 158, A343-A351.
59 A. Lewera, J. Inukai, W. P. Zhou, D. Cao, H. T. Duong, N. Alonso-Vante and A. Wieckowski, *Electrochimica Acta*, 2007, 52, 5759-5765.
60 P. K. Babu, A. Lewera, J. H. Chung, R. Hunger, W. Jaegermann, N. Alonso-Vante, A. Wieckowski and E. Oldfield, *Journal of the American Chemical Society*, 2007, 129, 15140-15141.
61 D. X. Cao, A. Wieckowski, J. Inukai and N. Alonso-Vante, *J. Electrochem. Soc.*, 2006, 153, A869-A874.
62 D. B. Sepa, M. V. Vojnovic and A. Damjanovic, *Electrochimica Acta*, 1981, 26, 781-793.
63 N. M. Markovic, H. A. Gasteiger and P. N. Ross, *The Journal of Physical Chemistry*, 1995, 99, 3411-3415.
64 H. Baltruschat, S. Ernst and N. Bogolowski, in *Catalysis in Electrochemistry*, ed. E. Santos and W. Schmickler, Wiley, 2011, pp. 297-337.
65 R. R. Adžić and J. X. Wang, *The Journal of Physical Chemistry B*, 1998, 102, 8988-8993.
66 V. Viswanathan, H. A. Hansen, J. Rossmeisl and J. K. Nørskov *The Journal of Physical Chemistry Letters*, 2012, 3, 2948-2951.
67 B. D. McCloskey, R. Scheffler, A. Speidel, D. S. Bethune, R. M. Shelby and A. C. Luntz, *Journal of the American Chemical Society*, 2011, 133, 18038-18041.
68 J. X. Wang, N. S. Marković and R. R. Adžić, *Colloids and Surfaces A: Physicochemical and Engineering Aspects*, 1998, 134, 165-171.
69 T. Abe, G. M. Swain, K. Sashikata and K. Itaya, *J. Electroanal. Chem.*, 1995, 382, 73-83.
70 A. J. Appleby, J. O. M. Bockris, E. B. Budevski, B. E. Coneway, A. R. Despic, R. R. Dogonadze, M. Enyo, D. Inman, S. U. M. Khan, L. I. Krishtalik, A. M. Kuznetsov, D. G. Lovering, R. Memming, E. J. Judd, A. Sadkowski, M. R. Tarasevich and E. Yeager, *Kinetics and Mechanism of Electrode Processes*, Plenum Press, New York, 1983.
71 R. R. Adžić, N. M. Marković and V. B. Vešović, *Journal of Electroanalytical Chemistry and Interfacial Electrochemistry*, 1984, 165, 105-120.
72 R. R. Adžić and N. M. Marković, *Journal of Electroanalytical Chemistry and Interfacial Electrochemistry*, 1982, 138, 443-447.
73 S. Ayata, A. Stefanova, S. Ernst and H. Baltruschat, *J. Electroanal. Chem.*, 2013, 701, 1-6.

74 A. Stefanova, S. Ayata, A. Erem, S. Ernst and H. Baltruschat, *Electrochimica Acta*, 2013, 110, 560 - 569.
75 T. Yano, E. Popa, D. A. Tryk, K. Hashimoto and A. Fujishima, *J. Electrochem. Soc.*, 1999, 146, 1081-1087.
76 A. Kraft, *International Journal of Electrochemical Science*, 2007, 2.
77 S. K. Si and A. A. Gewirth, *The Journal of Physical Chemistry B*, 2000, 104, 10775-10782.
78 F. G. Bordwell, *Accounts of Chemical Research*, 1988, 21, 456-463.
79 A. Khetan, A. Luntz and V. Viswanathan, *The Journal of Physical Chemistry Letters*, 2015, 6, 1254-1259.
80 Y. Marcus, *Chemical Society Reviews*, 1993, 22, 409-416.